I have reviewed this document and have found no classification issues.
M J Fagan 12/21/12
M J Fagan

Project Summary Report, NMSBA Muleshoe Engineering

Marion .W. Vance, AET-1
Los Alamos National Laboratory

December 2012

1 Background

This report describes a study of the fluid flow properties through a vessel designed to extract natural gas from a mixed multiphase inflow stream of liquid and gas. From here on, the gas and liquid are treated as calorically perfect methane and pure water, respectively. Similar to concept of hydrocyclones, a single liquid-gas stream enters the cylindrical device in a tangential trajectory, where gravity and centripetal accelerations contribute to separate the fluids of vastly different densities. The phase separation and distribution are further enhanced in this case by a double walled inflow tank and feedback control of the outflow. A drawing of the vessel is provided in figure 1. In very general terms, the device consists of a double-walled cylindrical tank at the bottom. Concentric to the inner radius is a tall central stack. The phase mixture of gas and liquid enters the outer annulus of the tank. The individual phases are subsequently evacuated through the distinct outlet systems each with feedback controlled motor-driven valves. The liquid water exits through two inch piping near mid-height. The methane gas exits from the top of the stack through nominal one inch piping. For the analysis of standard operating conditions as introduced in this report, all bypass and safety relief valves are ignored.

For the purpose of analysis, the device operation is split into two distinct processes. The phase separation discussed in section 3 occurs in the lower tank and is simulated with a full three-dimensional, time-dependent model. After separation, the individual phases are expelled through a cyclic process discussed in section 2, where a one-dimensional (time only) thermodynamic analysis is applied to control volume consisting of the central stack.

2 Control volume analysis

This section will describe the preliminary analysis of the gas processing cycle. See figure 2 for a diagram of the control volume. Throughout this analysis, we prescribe these assumptions. Inflow mass flow rates are known and constant. Inflow temperature is also fixed at T_i. The water system pressure P_{set} is controlled by the back pressure valve, and the operation of this device is idealized. The valve is assumed to have full authority for all operating conditions explored here, and its response is treated as immediate, consistent, and precise. A consequence of this assumption is a constant (and known) pressure across the expansion process. In contrast to that controller, the gas outflow valve is not immediate but instead has a open/close time constant of $\tau_v = 3\,\mathrm{s}$. Otherwise,

Project Summary Report, NMSBA Muleshoe Engineering

Marion .W. Vance, AET-1
Los Alamos National Laboratory

December 2012

1 Background

This report describes a study of the fluid flow properties through a vessel designed to extract natural gas from a mixed multiphase inflow stream of liquid and gas. From here on, the gas and liquid are treated as calorically perfect methane and pure water, respectively. Similar to concept of hydrocyclones, a single liquid-gas stream enters the cylindrical device in a tangential trajectory, where gravity and centripetal accelerations contribute to separate the fluids of vastly different densities. The phase separation and distribution are further enhanced in this case by a double walled inflow tank and feedback control of the outflow. A drawing of the vessel is provided in figure 1. In very general terms, the device consists of a double-walled cylindrical tank at the bottom. Concentric to the inner radius is a tall central stack. The phase mixture of gas and liquid enters the outer annulus of the tank. The individual phases are subsequently evacuated through the distinct outlet systems each with feedback controlled motor-driven valves. The liquid water exits through two inch piping near mid-height. The methane gas exits from the top of the stack through nominal one inch piping. For the analysis of standard operating conditions as introduced in this report, all bypass and safety relief valves are ignored.

For the purpose of analysis, the device operation is split into two distinct processes. The phase separation discussed in section 3 occurs in the lower tank and is simulated with a full three-dimensional, time-dependent model. After separation, the individual phases are expelled through a cyclic process discussed in section 2, where a one-dimensional (time only) thermodynamic analysis is applied to control volume consisting of the central stack.

2 Control volume analysis

This section will describe the preliminary analysis of the gas processing cycle. See figure 2 for a diagram of the control volume. Throughout this analysis, we prescribe these assumptions. Inflow mass flow rates are known and constant. Inflow temperature is also fixed at T_i. The water system pressure P_{set} is controlled by the back pressure valve, and the operation of this device is idealized. The valve is assumed to have full authority for all operating conditions explored here, and its response is treated as immediate, consistent, and precise. A consequence of this assumption is a constant (and known) pressure across the expansion process. In contrast to that controller, the gas outflow valve is not immediate but instead has a open/close time constant of $\tau_v = 3\,\mathrm{s}$. Otherwise,

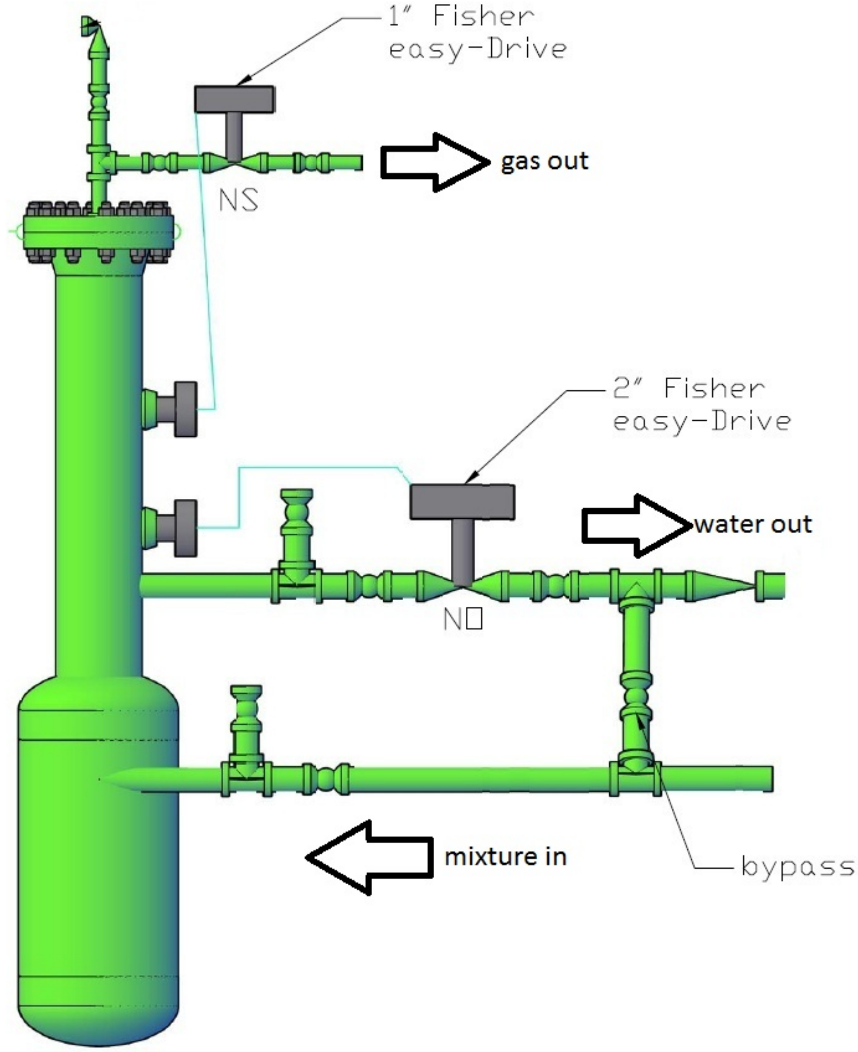

Figure 1: Graphical depiction with piping and valves

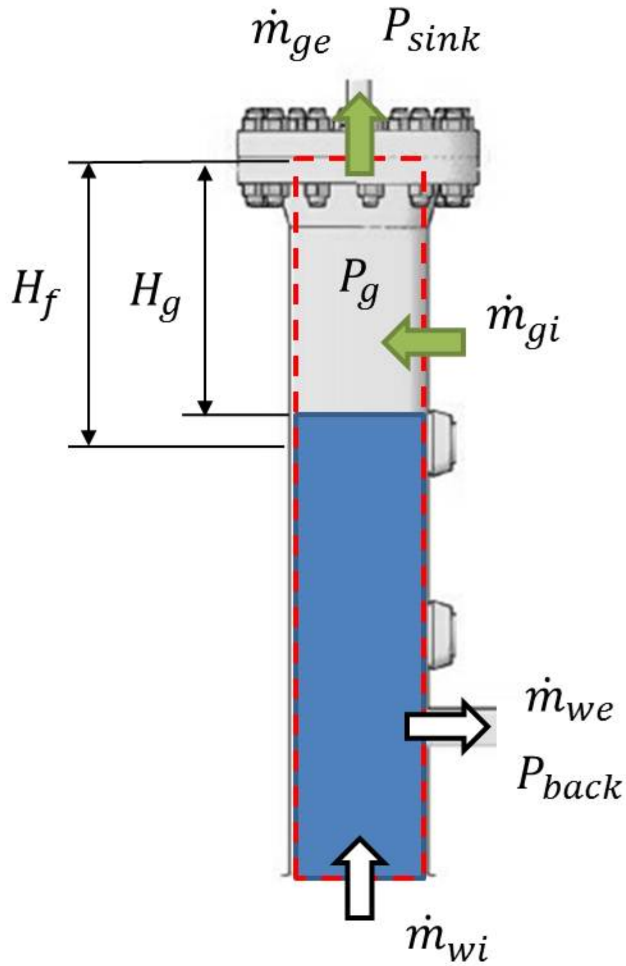

Figure 2: Control volume model of stack

the modeled response, including the float-valve actuation, is treated as perfect. The float valve is actuated by the liquid-gas interface $H_g(t)$ in the central stack. Between the open (down) and close (up) positions of the upper float valve, there is a known linear travel of $\delta_f = 3.5\,\text{in}$. The gas outflow is signaled to open at $H_g = H_f + 0.5\delta_f$ and receives the close signal where $H_g = H_f - 0.5\delta_f$. While H_g is the actual physical representation, it is the gas volume V_g that is directly modeled in the governing equations described below. Because the stack geometry is cylindrical, the variables H_g and H_f are directly proportional to their respective model values V_g and V_f.

Defined by the toggle of sensor states, there are three distinctly identifiable states in the idealized cycle. Those states are listed in table 1 in terms of the gathered gas volume $V_g = AH_g$ and pressure P_g in relation to the individual valve toggle values, P_{set} and V_f. Listed in table 2 are the distinct processes that produce the transition between each of states points. Although we refer to the sequence of processes as a *cycle*, we note that the final state (State 1*) may not be identical to the initial state (State 1). The valve states given in the table represent predicted conditions over the

State	P_g	V_g
1	$P_g \cong P_{set}$	$V_g = V_f^+$
1	$P_{sink} \leq P_g < P_{set}$	$V_g = V_f^-$
2	$P_g = P_{set}$	$V_g < V_f$

Table 1: Definition of states

Label	From state	To state	Description	gas valve	water valve
I	1	2*	gas purge	open	shut
II	1	2	gas compression	shut	shut
III	2	3	gas expansion	shut	open

Table 2: Definition of processes

bulk of each process. However, there is considerable overlap as the individual valves open and close during the state transitions. The coupling of the feedback operation brings sufficient complexity, even to this greatly simplified control volume, to preclude a purely analytical treatment. Instead, the process models introduced in the following sections are numerically integrated.

2.1 Governing equations

For simplicity, we can begin with a simplified one-dimensional model with time as the only independent variable. Fluid interactions within the stack are neglected. By treating the liquid phase as incompressible, a pair of equations for the volume V_g and mass m_g of the gathered gas can be written directly from conservation of mass.

$$\frac{dV_g}{dt} = \frac{\dot{m}_{we} - \dot{m}_{wi}}{\rho_w} = q_{we} - q_{wi} \tag{1}$$

$$\frac{dm_g}{dt} = \dot{m}_{gi} - \dot{m}_{ge} \tag{2}$$

In equation (1), $q \equiv \dot{m}/\rho$ is the volume flow rate. From the ideal gas equation of state, the *absolute* gas pressure P_g inside the stack can then be written with the closed forms of V_g and m_g.

$$P_g = RT\frac{m_g}{V_g} \tag{3}$$

Also, the processes are assumed polytropic where appropriate, and that provides an in-process relationship between gas pressure and density.

$$P_g\left(\frac{V_g}{m_g}\right)^{\gamma} = \text{cst} \tag{4}$$

The exponent of (4) is set to $\gamma = 1$ for an isothermal constraint, or $\gamma = k$ for isentropic. Intermediate values of γ ($1 \leq \gamma \leq k$) are typically observed in experimental tests, but any significant heat transfer would make the values for each process difficult to predict.

2.2 Gas outflow relations

Although strictly derived for steady flow, the mechanical energy equation can provide an appropriate estimate of a variable outflow rate for our purposes. Ignoring changes in potential energy and the "reservoir" velocity, we can rearrange the equation to isolate the average exit velocity in terms of the pressure drop.

$$\overline{u}^2 = C^2 \left(\frac{P_o - P}{\rho} \right) \tag{5}$$

The discharge coefficient C combines the major and minor losses of the flow through the exit piping, valves, and fittings. Expressed with the typical terms of head loss values in pipe equations, it has the form

$$C^2 = 2 \left[1 + \frac{fL}{d} + \Sigma K_m \right]^{-1} . \tag{6}$$

The Darcy friction factor f, while actually weakly dependent on the velocity $\overline{u}$, is treated as a constant here. It and the remaining terms (pipe length L, pipe diameter d, and individual minor losses K_m) are simply lumped together, and a single representative value is assigned to C. For our current purposes, C serves as a simulation tuning parameter. Later, it could be calibrated with comparison to measured data or empirical values provided by hydraulic handbooks and pipe manufacturing data. In the above, P_o is the "reservoir" (vessel) pressure, which will be set equal to P_g for most calculations, and P represents some yet to be identified downstream pressure. From (5), an expression for a mass flow rate exiting the vessel can be written as

$$\dot{m} = CA\sqrt{\rho |P_o - P|} \tag{7}$$

where A and C represent the average area and discharge coefficient through the relevant exit piping system. Somewhere downstream of the exit, valves, and fittings, we must eventually assume a system back pressure P that provides the pressure drop to drive the outflow.

The compressibility of the gas and the likelihood of choked conditions must be accounted for during the gas purge process. For a given value of P_{sink}, the following expression gives an estimate for the pressure ratio for choked flow through the exit valve.

$$\frac{P_g^*}{P_{sink}} = \left(\frac{k+1}{2} \right)^{k/(k-1)} \tag{8}$$

The above relation treats the gas as calorically perfect with specific heat ratio k and is derived for an isentropic exit through a well-designed converging nozzle. Applying a value of $k = 1.3$ for methane, the right hand side of (8) evaluates to 1.8. In comparison to the expected working pressure range in the vessel, we expect the flow to be choked for most, if not all, of the gas purge process. Holding the assumption of isentropic flow of a calorically perfect gas, the following expression provides the mass flow rate during choked flow.

$$\dot{m}_{ge} = \upsilon C_g A_g \sqrt{\rho_g P_g k \left(\frac{2}{k+1} \right)^{\frac{k+1}{k-1}}} \qquad \text{for } P_g \geq P_g^* \tag{9}$$

The constants C_g and A_g represent the gas discharge coefficient and average exit area. For gas pressure below the choke value, the mass flow rate is given by rewriting equation (7) with our gas notation.

$$\dot{m}_{ge} = \upsilon C_g^* A_g \sqrt{\rho_g |P_g - P_{sink}|} \qquad \text{for } P_g < P_g^* \tag{10}$$

In the above, υ represents the gas valve open ratio. It and C_g^* are discussed below. The discharge coefficient C_g in the choked flow equation (9) serves as the single simulation tuning parameter for the gas outflow.

The gas release valve moves from fully closed to fully open in $\tau_v = 3\,\mathrm{s}$. For simplicity a linear ratio is imposed, and the valve opening ratio $\upsilon(t)$ is a simple ramp function of positive slope if opening and negative if closing. The open/close events are toggled by the float switch actuated by gas volume transition between V_f^+ and V_f^-.

$$\upsilon(t) = \begin{cases} \upsilon_0 + (t - t_0)/\tau_v & V_g(t_0) = V_f^+ \\ \upsilon_0 - (t - t_0)/\tau_v & V_g(t_0) = V_f^- \end{cases} \tag{11}$$

The value saturates at either zero or unity, $0 \leq \upsilon \leq 1$, for fully closed or fully opened states, respectively. See figure 7 for a graphical description of a typical rise-fall signal of $\upsilon(t)$.

The value of the unchoked gas discharge coefficient C_g^* is fixed by ensuring continuity of $\dot{m}_{ge}$ across the transition from choked to unchoked flow. Equating (9) and (10) with $P_g = P_g^*$ yields the following expression for C_g^*.

$$C_g^* = C_g \left[\frac{k\left(\frac{2}{k+1}\right)^{1/(k-1)}}{\left(\frac{k+1}{2}\right)^{k/(k-1)} - 1} \right]^{1/2} \approx C_g \tag{12}$$

Plugging in the value of $k = 1.3$ for methane gas, we calculate $C_g^* = 0.99 C_g$ and determine that $C_g^* \approx C_g$ can be applied with negligible discontinuity in the transition from choked flow.

2.3 Liquid outflow relations

The liquid outflow is controlled by a check valve and back-pressure valve in series. During the expansion process, from State 2 to State 3, the pressure is held constant at P_{set} by the back-pressure valve through the release of liquid mass from the control volume. Directly from the ideal gas equation of state, we can write a relation for the gas volume during the expansion process ($\dot{m}_{ge} \approx 0$).

$$V(t) = V_2 + \frac{\dot{m}_{gi} R T_2}{P_{set}}(t - t_2) \qquad t_2 \leq t \leq t_3 \tag{13}$$

Under the polytropic model, the density and temperature of an ideal gas during a constant pressure process are also constant, and the substitution $\rho_2 = \rho_3 = P_{set}/RT_2$ has been made in the above expression. Taking the derivative of $V(t)$ as given by (13) and replacing the left side of the differential equation (1) yields an expression for the nominal value of the exit water volume flow rate.

$$q_{we}^* = q_{wi} + \frac{\dot{m}_{gi} R T_2}{P_{set}} \tag{14}$$

The expression for q_{we}^* represents the water outflow required to maintain a constant pressure of P_{set}. In the derivation of (15), there is an implicit assumption that the initial pressure is $P_2 = P_{set}$, which is the mathematical equivalent of a perfect check valve that instantaneously opens at P_{set}. If the check valve is cracked open at a pressure P_c substantially different than P_{set}, a simple proportional control is applied in the following manner.

$$q_{we} = q_{we}^*(1 + K_w \epsilon) \qquad \text{where} \quad \epsilon = P_g - P_{set} \tag{15}$$

The proportional control model is an appropriate estimate for a spring activated device like the back-pressure valve. A quick inspection of equation (15) verifies that the model properly mimics the intent of the back-pressure valve. For positive (negative) values of ϵ, the outflow is increased (decreased) in effort to decrease (increase) the upstream pressure. For sufficiently low vessel pressure $P_g < P_{set}$, the check valve closes and negative values of q_{we} are avoided. Where $\epsilon = 0$, the valve makes no adjustment and flows at the preset stability point. The constant K_w is a simulation tuning parameter and requires comparison to measurements or other empirical data for proper evaluation. We can also specify $K_w = 0$ for a simplified model and/or a non-feedback operation.

2.4 Numerical integration

The pair of ordinary differential equations, (1) and (2), combined with the algebraic equations of state (3) and (4), constitute the complete set of governing equations for the 1-d control volume analysis. In the physical and mathematical senses, the system is driven by the source terms on the right hand sides of (1) and (2). For both fluids, the mass inflow rates do not vary with time. The underlying phase separation is also assumed to be steady and complete. Thus, the source terms q_{wi} and $\dot{m}_{gi}$ in equations (1) and (2) are held constant across the entire cycle. In contrast, the separate mass flows out of the control volume are functions of the time-varying gas pressure P_g and are independently controlled though valve open/shut events at the distinct states listed in table 1. Depending on the process, the appropriate combination of equations (9), (10), (15) is applied. The cycle is initiated at arbitrary values of P_g and V_g and integrated forward in time using a second-order explicit method. For the standard operating conditions applied in these evaluations, the process evolves into a complete cycle within a couple periods. In all cases, the process is allowed to evolve for several cycles and statistics are taken over the final complete cycle. The periodic cycle is independent of the initial conditions.

2.5 Numerical Results

For simplicity and ease of comparison, the temperature of all processes is held constant (*i.e.* $\gamma = 1$) and set to the inflow mixture value, $T(t) = T_i = 80^o\,\mathrm{F}$. As mentioned in the previous section, the mass inflow rates do not vary with time for these simulations, but we run multiple cases to examine the influence of those values. Unless otherwise noted, the following values are applied throughout this section, $C_g = 0.1$, $K_w = 0$, $\tau_v = 3\,\mathrm{s}$, and $P_{sink} = 35\,\mathrm{psig}$. The corresponding choke pressure from equation (8) is $P^* = 77\,\mathrm{psig}$. It should be noted that while the pressure values are reported as gauge and in units of psi, the relations described in the previous sections require absolute pressure and temperature values in SI units. Finally, we emphasize that the parameters C_g and K_w have been set to arbitrary values with no attempts made at calibration or optimization. As such, all reported results should be treated as preliminary at best, where the goals of this preliminary investigation are limited to identifying trends.

2.5.1 Baseline values

A baseline inflow setting is arbitrarily selected with $q_{wi} = 1000\,\mathrm{bbl/day}$ and $q_{gi} = 10\,\mathrm{MSCF/day}$. The following pressure values are also baseline selections, $P_{set} = 200\,\mathrm{psig}$ and $P_c = P_{set} + 2\,\mathrm{psi}$. The gas pressure evolution for a complete cycle is shown in figure 3. The selected start point of the cycle (*i.e.* reference $t = 0$) is the gas valve open trigger, *i.e.* $V(0) = V_f^+$. The observed

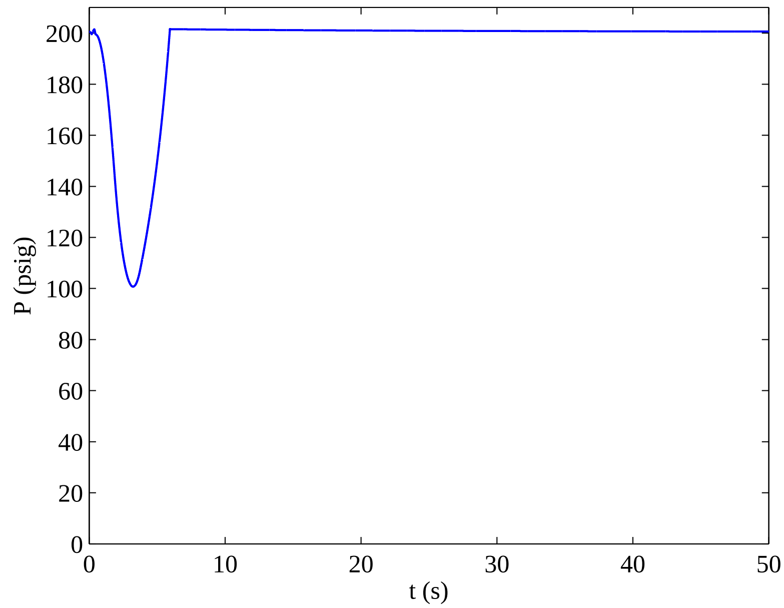

Figure 3: Baseline parameters, cycle gas pressure transient

cycle duration is 50.5 seconds. The predicted gas outflow remains choked with these baseline parameters. Figure 4 shows the gas-liquid interface level H_w as measured from the float open position, $H_f^+ = H_f + 0.5\delta_f$. Although the dependent variable in the governing equations is actually gas volume $V(t)$, the interface level H_w is reported because it is easy to reference and exactly but indirectly proportional. By definition, the cycle is initiated at the purge process triggered by $H_w(0) = 0$ as shown in figure 4. During the purge process and overlapping into compression, H_w increases (V decreases) because $q_{we} = 0$. When $P(t)$ again builds to the water valve system cracking pressure P_c, water flows out and H_w drops linearly to zero, upon which the cycle repeats.

Using the same results, this axis limits are tightened to focus on the purging process in figures 5-8. The pressure shown in figure 5 oscillates slightly at the onset of the valve opening. This is not a numerical artifact but is instead a result of the modeled behavior of the check and back-pressure valves. Because P drops immediately at $t = 0$, the water check valve instantly closes causing H_w and consequently P to reverse gradient and build. This back and forth competition continues until sufficient gas outflow is attained to drop the pressure. The corresponding evolution of gas valve open ratio υ and gas volume outflow rate are shown in figures 7 and 8, respectively. During testing, the check valve was also modeled with some delay/damping, but the changes in overall results (*e.g.* $\min(P)$) were not significant unless a seemingly unphysical long delay was applied.

If the short duration between $t = 0$ and the complete closing of the water system check valve is neglected, an estimation of the purge process time span (from open signal to close signal) is easily attained from the exact solution of equation (1) with $q_{we} = 0$.

$$t_1 = \frac{V_f^+ - V_f^-}{q_{wi}} \tag{16}$$

Using relation (16) and the input parameters, an estimate of $t_1 = 1.6\,\mathrm{s}$ is calculated. The actual

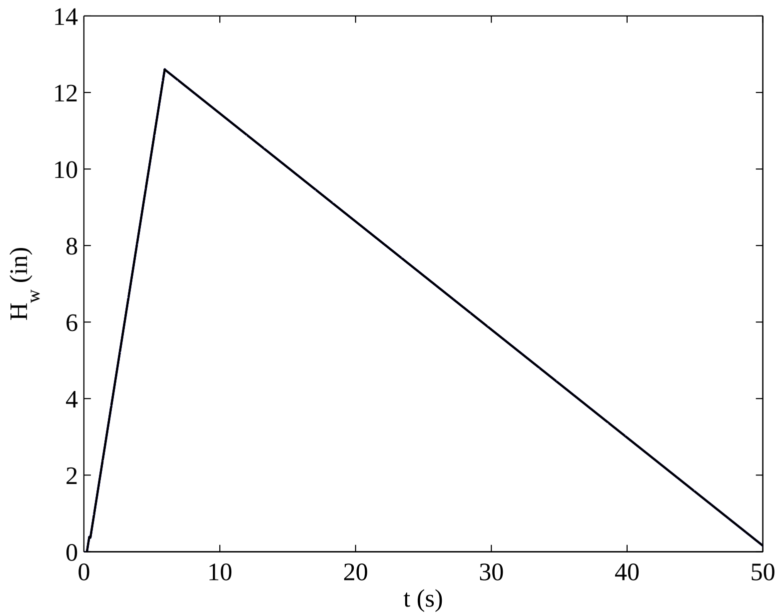

Figure 4: Baseline parameters, cycle gas-liquid level transient

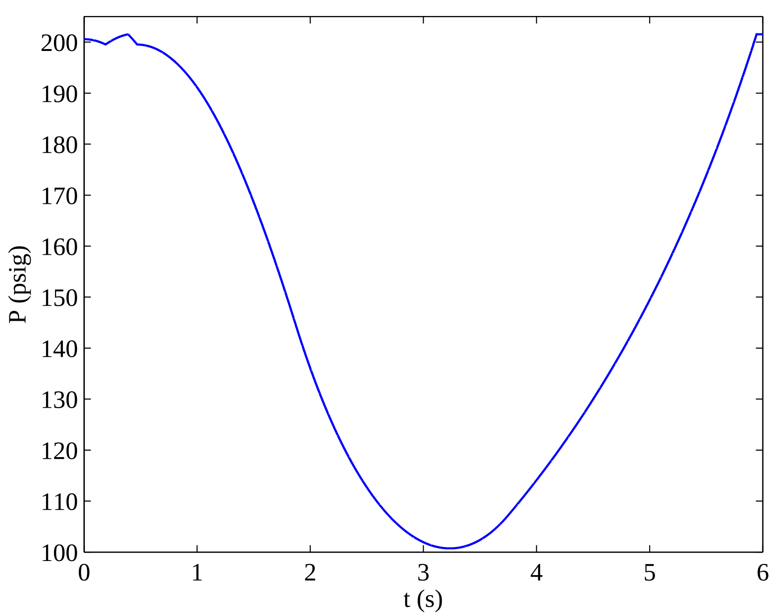

Figure 5: Baseline parameters, gas pressure during purge

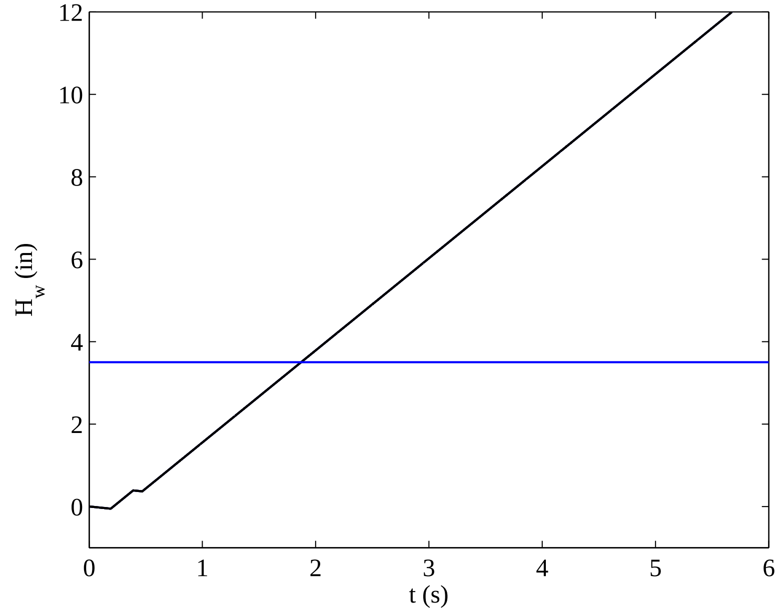

Figure 6: Baseline parameters, gas-liquid level during purge. Horizontal lines represent the on-off levels

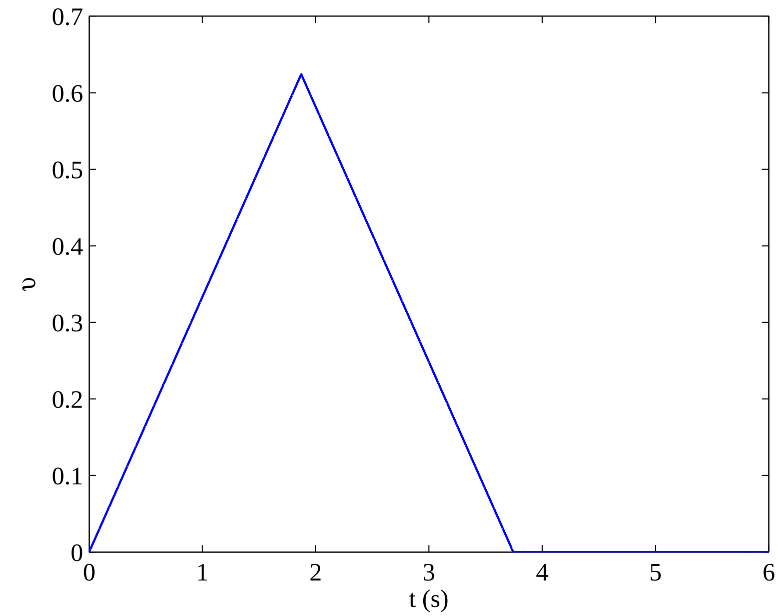

Figure 7: Baseline parameters, gas valve open ratio during purge

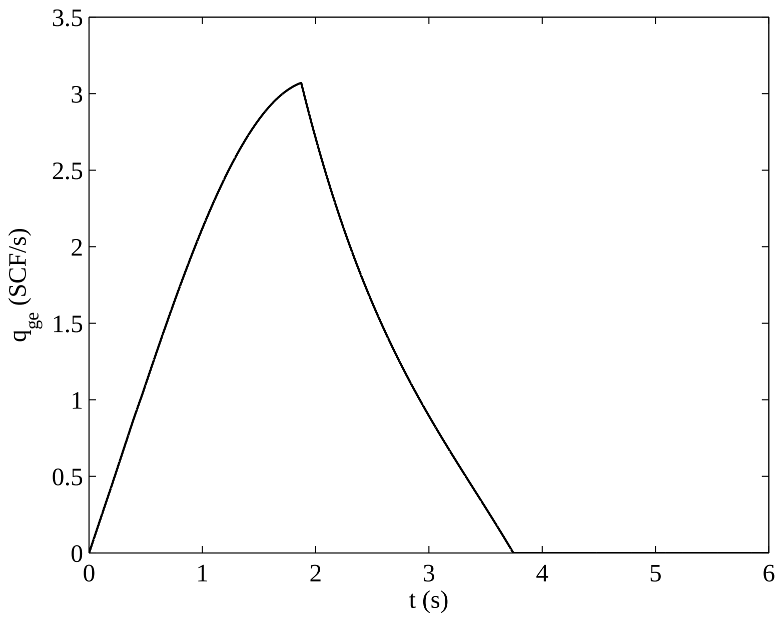

Figure 8: Baseline parameters, gas outflow during purge

value observed in the simulation is 1.9 s and depicted in the crossing shown in figure 6. It is worth remarking here that the values $(V_f^+ - V_f^-)$ and t_1 can be physically measured in operation, thus providing *in situ* approximations of q_{wi} through equation (16).

2.5.2 Influence of P_{set}

With the exception of increasing the set pressure by roughly two atmospheres to $P_{set} = 230\,\text{psig}$, all other parameters are held at the previously described baseline values. Figure 9 compares the pressure transients during the gas purging phase. While the set pressure was increased by fifteen percent, the difference between minimum pressure values is smaller at approximately ten percent. Otherwise, there is no significant variation in the pressure curves. With similar focus paid to the purge process, the gas outflow is shown in figure 10. Comparison of the two curves in that figures reveals that the increased pressure setting yielded a commensurate increase in peak outflow values. Although the duration of the purge process is relatively unchanged, more gas is processed out *per cycle* at the increased pressure setting.

If we integrate $\dot{m}_{ge}(t)$ over several cycles and normalize by the total time to determine an average rate, that value must match the constant inflow rate to satisfy mass conservation. Coupled with the assumption that the peak values in figure 10 provide some measure of the actual gas outflow, we expect the cycle duration should also increase. Figure 11 compares $H_w(t)$ for the two pressure settings, and the increase in cycle duration is apparent. Also evident in the the figure, the increase in cycle duration is predominantly due to the decrease in slope (magnitude) during the expansion process. Noting that

$$\frac{dV}{dt} = -\alpha \frac{dH_w}{dt} \,,$$

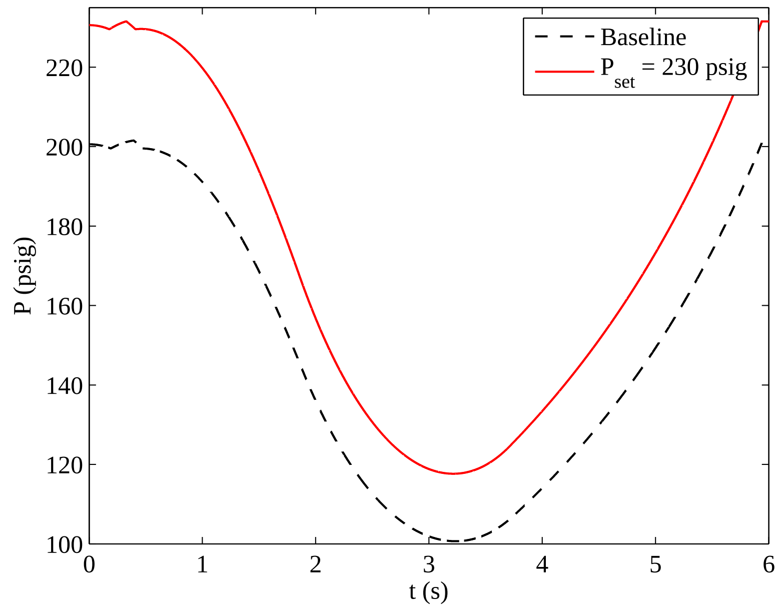

Figure 9: $P_{set} = 230\,\text{psig}$, gas pressure during purge

where the constant of proportionality α is given by the cross-section area of the central stack, we can determine an exact relation for that slope by substituting equation (15) into equation (1).

$$\frac{dH_w}{dt} = -\frac{RT_2}{\alpha}\left(\frac{\dot{m}_{gi}}{P_{set}}\right) \tag{17}$$

In arranging the above expression, we note that $q_{we} = q^*_{we}$, because $K_w = 0$ is applied here. Equation (17) clearly reveals that the rate of change of the interface level (or gas volume) is directly proportional to the ratio of the gas inflow and the pressure setting.

By varying P_{set} over a range of values, we can examine the effects on the cycle extrema. The minimum cycle pressure for several values of P_{set} is plotted in figure 12. The trend is a fairly linear increase with a slight jog around $P_{set} = 200\,\text{psig}$. For $P_{set} < 150\,\text{psig}$, the minimum pressures drop below the estimate choke pressure of $P^* = 77\,\text{psig}$. Figure 13 shows the peak gas outflow over the range of set pressure values, and the trend is also a linear increase. As mentioned above, mass conservation dictates a reflected increase in the cycle duration, and that results is demonstrated in figure 14. Similar to the minimum pressure, there is a noticeable jog about $P_{set} = 200\,\text{psig}$ in the plot shown in figure 14. The jog is explained, or least better displayed, by the the maximum H_w values plotted in figure 15. The range on the vertical axis is narrow to exaggerate the difference. Through examination of other simulation variables, the observed jump occurs closer to 190 psig and was determined to be a result of the modeled behavior of the water valve system. At the applied baseline inflow values, this pressure marks a distinction in the requirement of the simulated check valve to actuate multiple times at the onset of the gas purge.

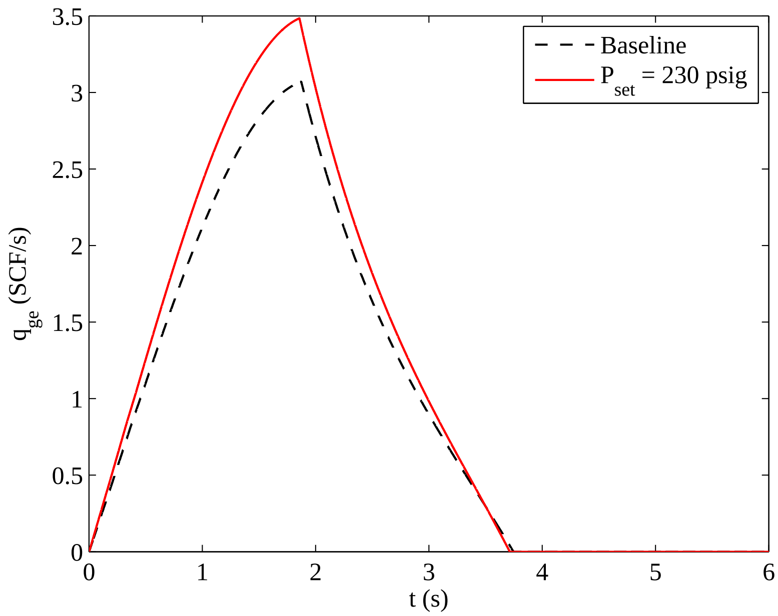

Figure 10: $P_{set} = 230\,\mathrm{psig}$, gas outflow during purge

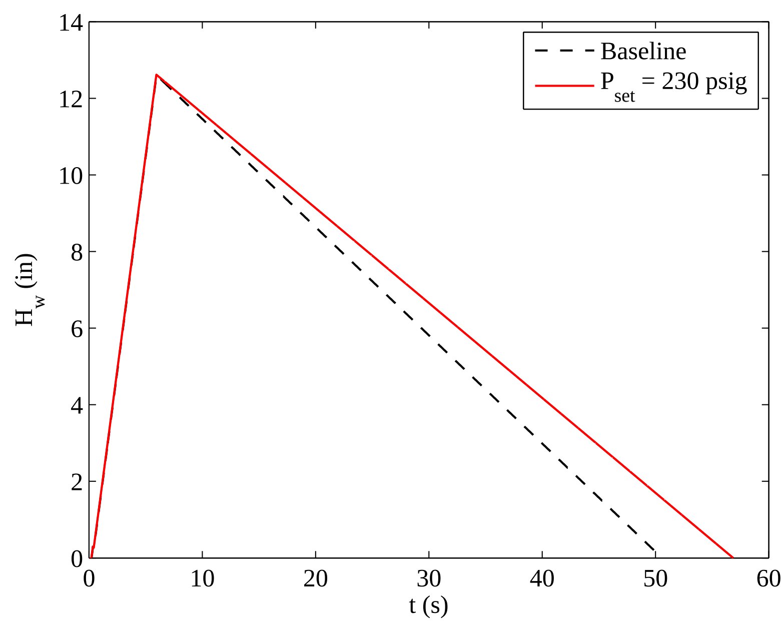

Figure 11: $P_{set} = 230\,\mathrm{psig}$, cycle gas-liquid level transient

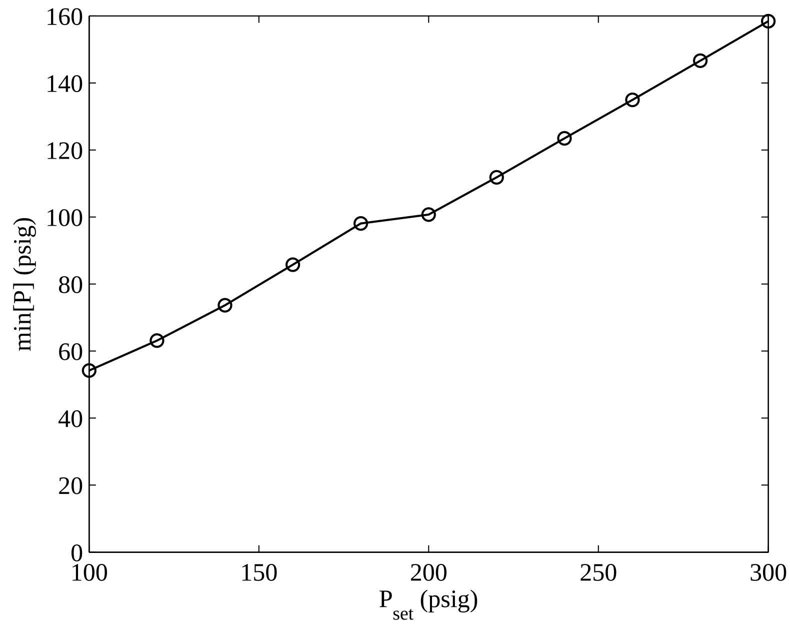

Figure 12: Baseline values with varied P_{set}, minimum cycle pressure

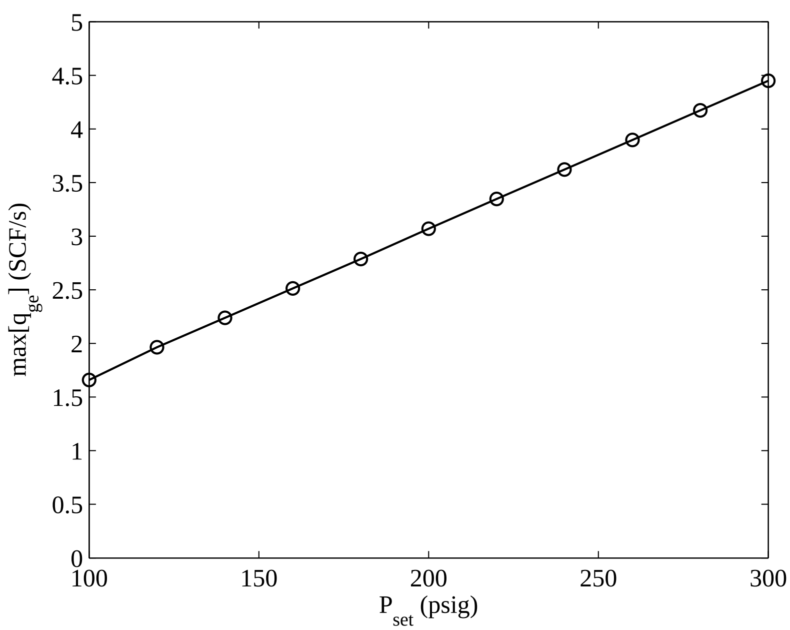

Figure 13: Baseline values with varied P_{set}, maximum cycle gas outflow

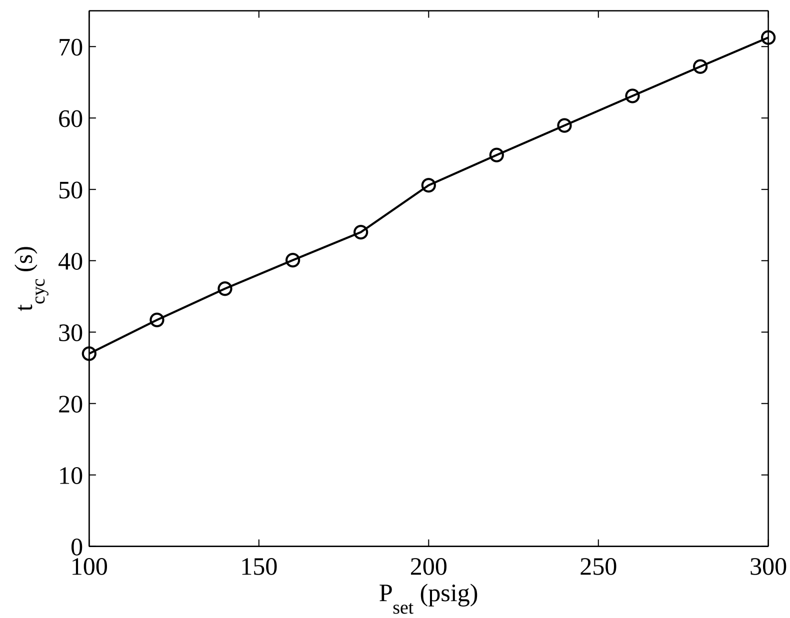

Figure 14: Baseline values with varied P_{set}, cycle duration

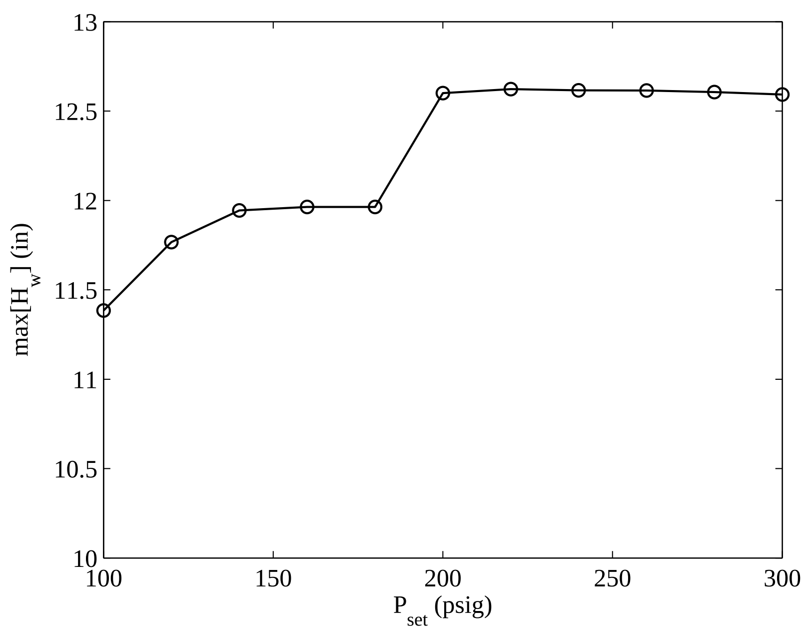

Figure 15: Baseline values with varied P_{set}, maximum H_w. Note nonzero values at origin.

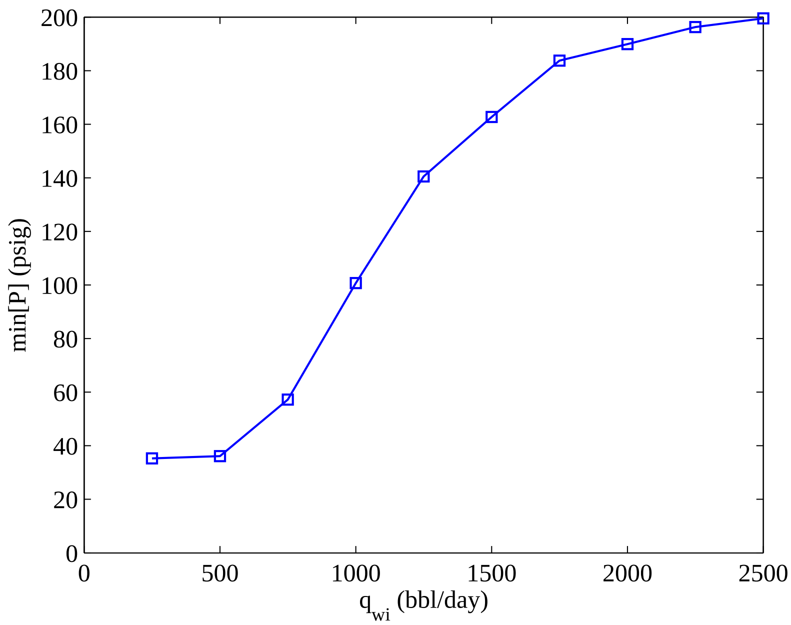

Figure 16: Baseline values with varied q_{wi}, minimum cycle pressure

2.5.3 Influence of q_{wi}

Here, P_{set} is reset and fixed to the baseline value of 200 psig. All other previously defined baseline parameters are applied, as well, with the exception of the water inflow rate. In this section, cycle extrema are compared for several different values of q_{wi}. The minimum cycle pressure curve is shown in figure 16. From inspection of the minimum pressures, we note that the purge process dips into unchoked flows for $q_{wi} < 1000\,\text{bbl/day}$. At the upper range of q_{wi}, the minimum value of P approaches P_{set}, at which point little or no gas is processed. Of course, without proper calibration of the applied models and tuning parameters, a great deal of care must be taken when interpreting the numerical results. The significance exhibited in figure 16, for example, is the indication that a minimum operating value of P_{set} may exist and is observed to be a function of the water inflow rate.

In figures 17 and 18, the cycle duration and maximum interface height both generally decrease with increasing water throughput. In the previous section, the influence of P_{set} was observed to have greatest impact during the expansion phase of the process. In contrast, equation (17) reveals that q_{wi} should have negligible effect during expansion. Instead, the influence of q_{wi} is upon the purge process, and some of this effect is directly evident in equation (16). Increased water flow shortens time span that the gas valve is opened. Effects of which are observed in the decaying trends in figures 17 and 18.

As previously discussed, the gas outflow per cycle will also increase in proportion to the cycle duration. The peak values of q_{ge} as plotted in figure 19 do not exactly follow that trend. Instead, the peak values decrease with decreasing water flow for $q_{wi} < 1000\,\text{bbl/day}$. Mass is still conserved, of course, and figure 19 only proves that the peak gas outflow values are poor indicators of total gas output. For example, the gas outflow transients for a few values of q_{wi} are compared in figure 20.

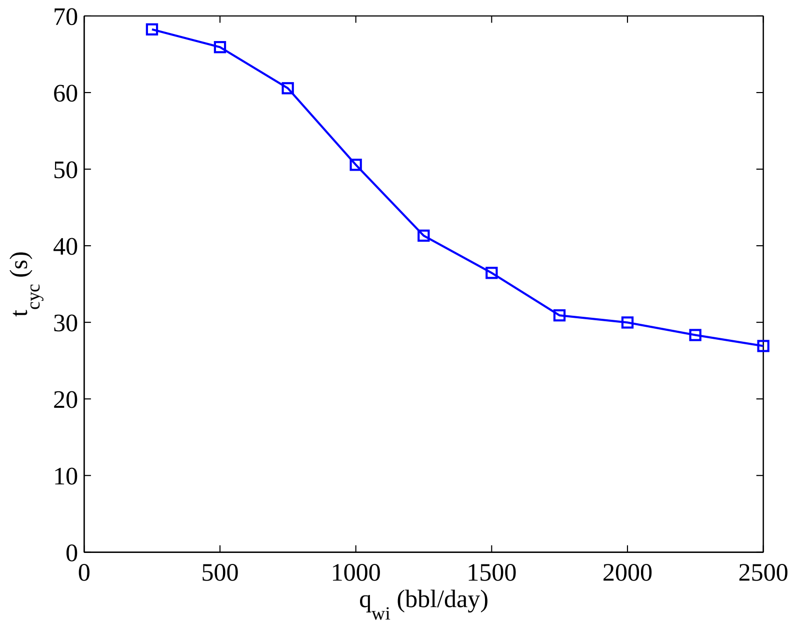

Figure 17: Baseline values with varied q_{wi}, cycle duration

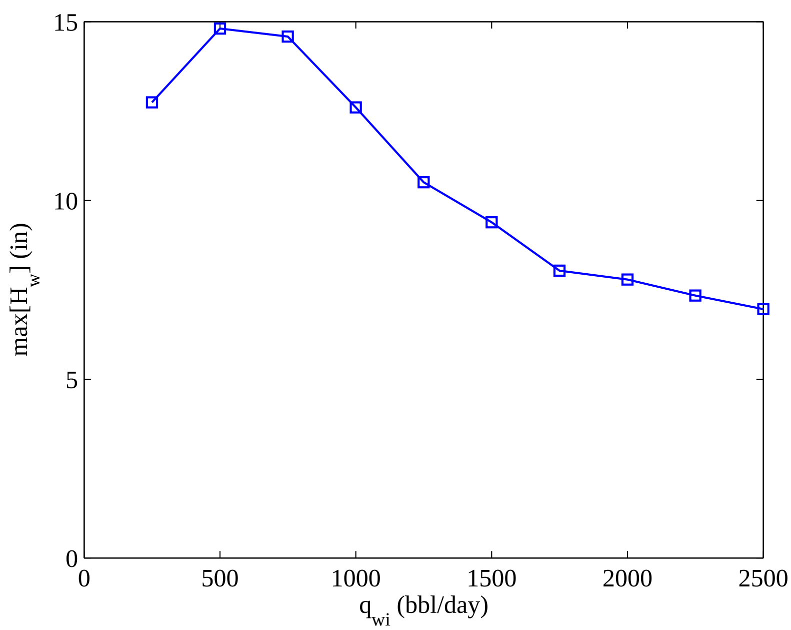

Figure 18: Baseline values with varied q_{wi}, maximum H_w.

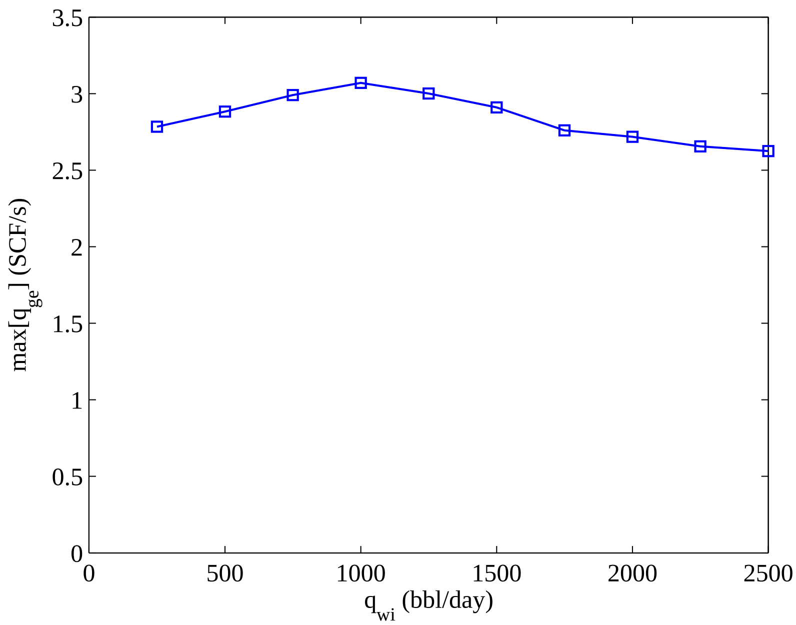

Figure 19: Baseline values with varied q_{wi}, maximum cycle gas outflow

As shown in the figure, the gas outflow curve for the lower water flow rate of 500 bbl/day is far from linear and far from symmetric, thus ruling out the use of peak value comparisons. At previously noted, the cycle duration is a sufficient indicator of gas processing per cycle.

2.5.4 Influence of $\dot{m}_{gi}$

Again, q_{wi} is reset and fixed to the baseline value of 1000 bbl/day. All other previously defined baseline parameters are applied, as well, with the exception of the gas inflow rate. Cycle extrema are compared for several different values of q_{gi}. The cycle duration shown in figure 21 decays rapidly with increasing gas inflow. Analogous to the variation in P_{set}, but in reciprocal effect, much of the impact on t_{cyc} is contained in the influence on the rate of change of the gas volume during the expansion process, *c.f.* equation (17). A direct effect of increased gas inflow is a proportional increase in the net water outflow during the expansion process, leading to shorter cycle times.

The minimum cycle pressure curve is shown in figure 16. The minimum pressure and maximum interface height shown in figure 23 are fairly consistent across the range of gas inflow. Both curves exhibit signs of gradient jumps, manifested by the ratcheting slopes. As with the single jog observed in the P_{set} curves (*c.f.* figure 15), the culprit is again multiple cycles of the check valve induced by our simplified model. The resulting oscillations are clearly visible in figure 24. Also apparent in the figure, increasing gas inflow increases the initial dwell time of the purge process, where the water valve system is still working to control the vessel pressure. Because the water valves remain open, the interface level continues to fall below the float open position (*i.e.* $H_w < 0$) as shown in figure 25. The gas outflow is unaffected by all of this and is basically colinear for the first second as shown in figure 26. The highest gas flow inflow rate also results in the outflow peaking prior to the valve beginning to close. As a reference, the gas valve open ratio went as high as 0.85 for

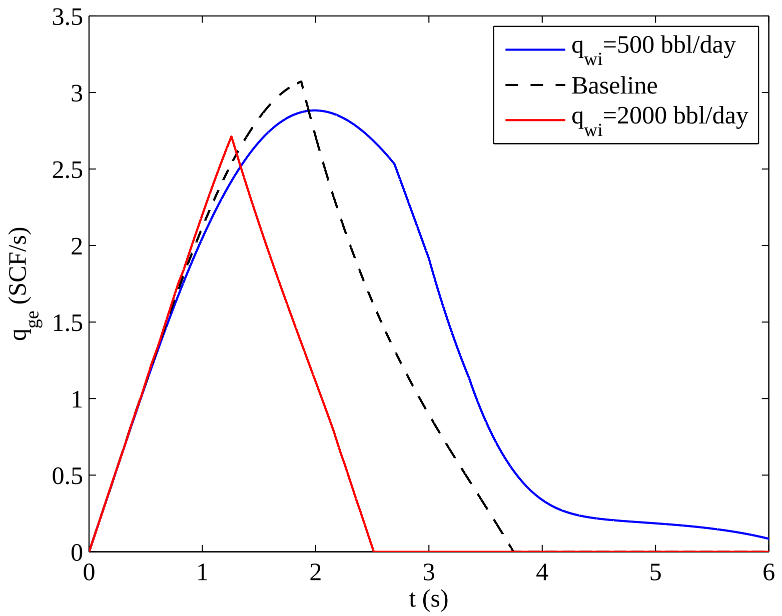

Figure 20: Baseline values with varied q_{wi}, gas outflow during purge

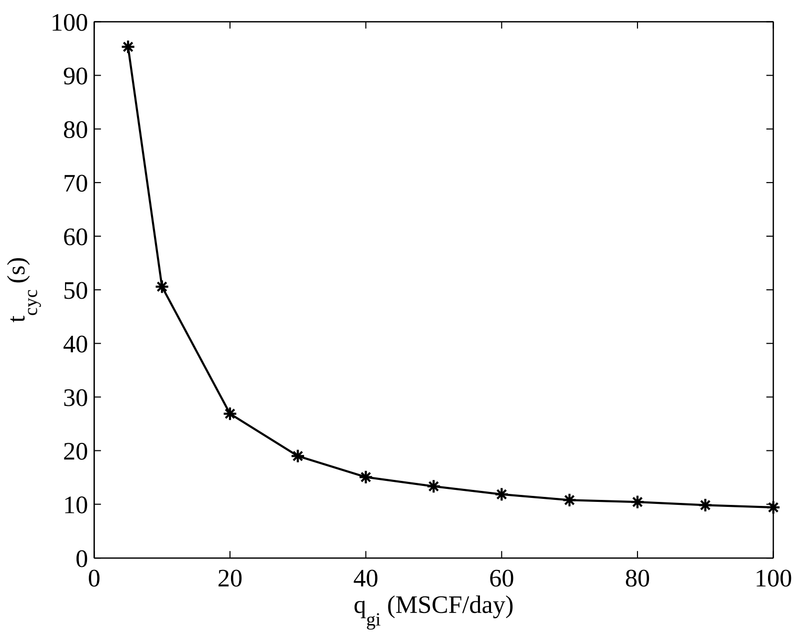

Figure 21: Baseline values with varied q_{gi}, cycle duration

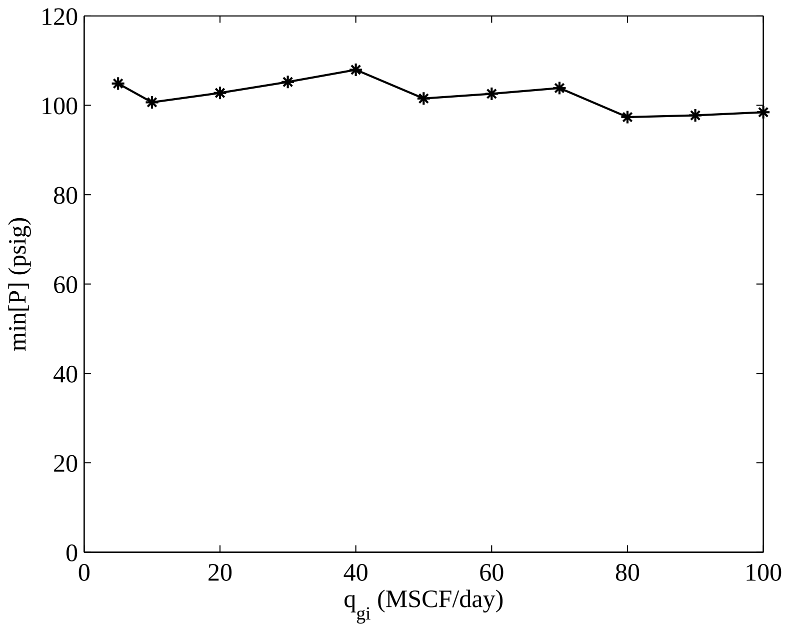

Figure 22: Baseline values with varied q_{gi}, minimum cycle pressure

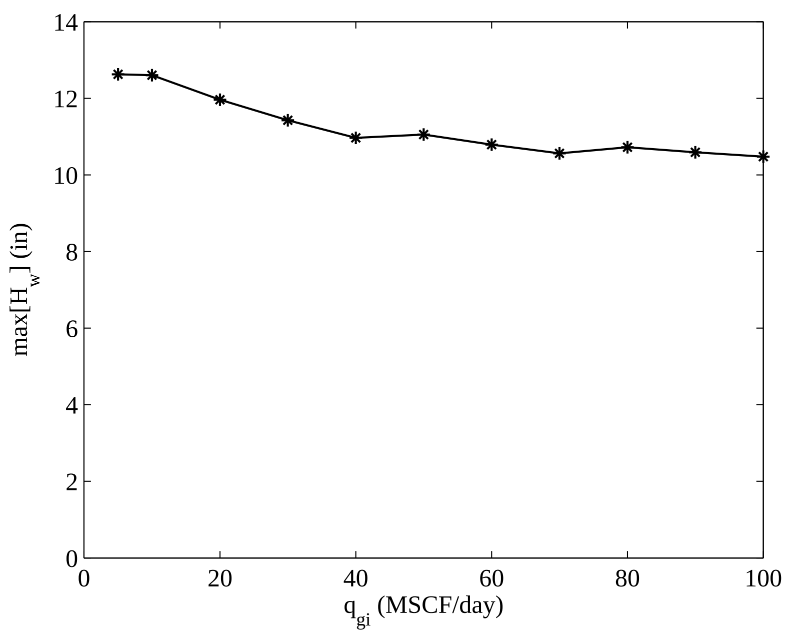

Figure 23: Baseline values with varied q_{gi}, maximum H_w.

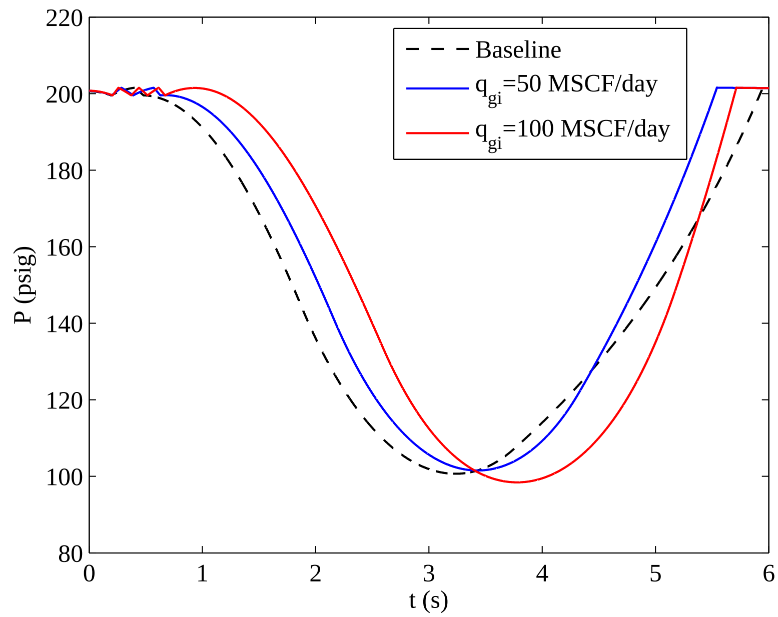

Figure 24: Baseline values with varied q_{gi}, gas pressure during purge

$q_{gi} = 100\,\mathrm{MSCF/day}$ result shown in figure 26.

2.5.5 Influence of C_g

In this section, the effects of the gas discharge coefficient are examined. Eventually, this parameter would need to be evaluated through comparison to known results. By making some blind adjustments here and checking the response, our goal is simply to verify that the previously observed trends are not signficantly affected. *A priori*, we know that the effects of C_g are limited to the gas purge process. From inspection of the mass discharge relations (9) and (10), the value of C_g acts as an efficiency multiplier for the gas purge. The direct effect is demonstrated by comparison of gas outflow curves shown in figure 27. The purging pressure response for a few representative values of C_g is plotted in figure 28. The enhanced mass flow leads to increased pressure drop. In fact, the minimum pressure is a likely candidate for selecting physical values of the coefficient. With increasing values of C_g, the pressure drop increases, which in turn causes a deeper compression fill. Figure 29 displays the increased volume change and corresponding cycle duration increase. Overall, there is no alarming sensitivity to the discharge coefficient, and the system influences discussed in the previous sections are expected to be preserved for a reasonable range of C_g.

3 Phase separation simulation

Towards the goal of investigating the multiphase flow in the outer compartment of the lower tank, we set up a CFD simulation in ANSYS CFX. The results presented here are again preliminary and have not been verified or validated. They are provided in the sense of proof of concept and motivation for further study. The basic geometry of the simulation model is shown in figure 30. In

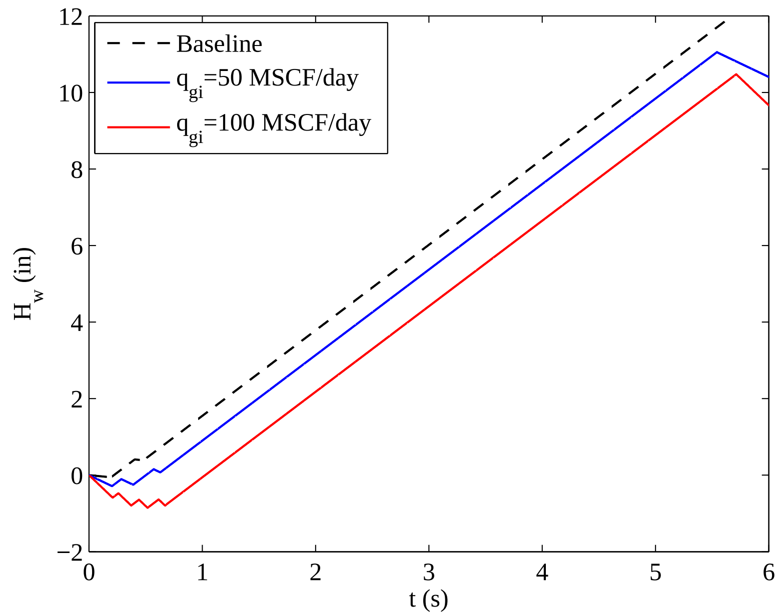

Figure 25: Baseline values with varied q_{gi}, gas-liquid level during purge

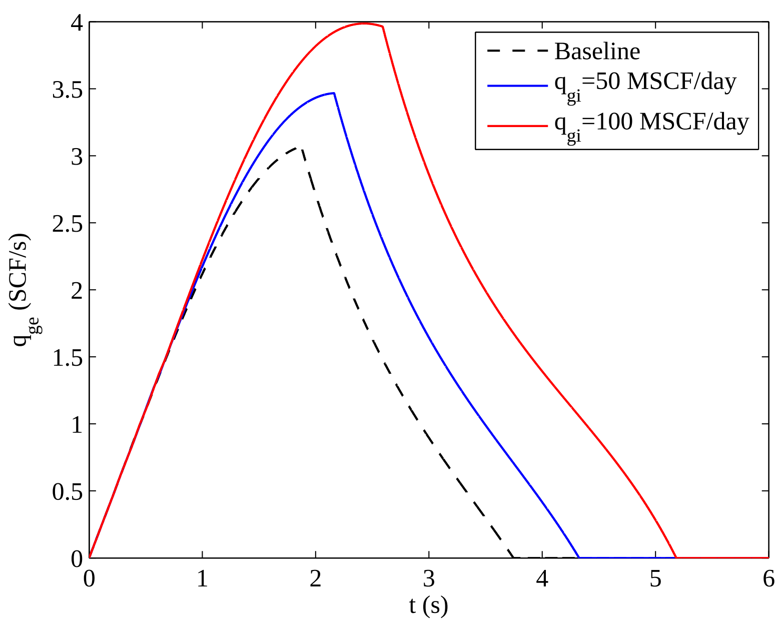

Figure 26: Baseline values with varied q_{gi}, gas outflow during purge

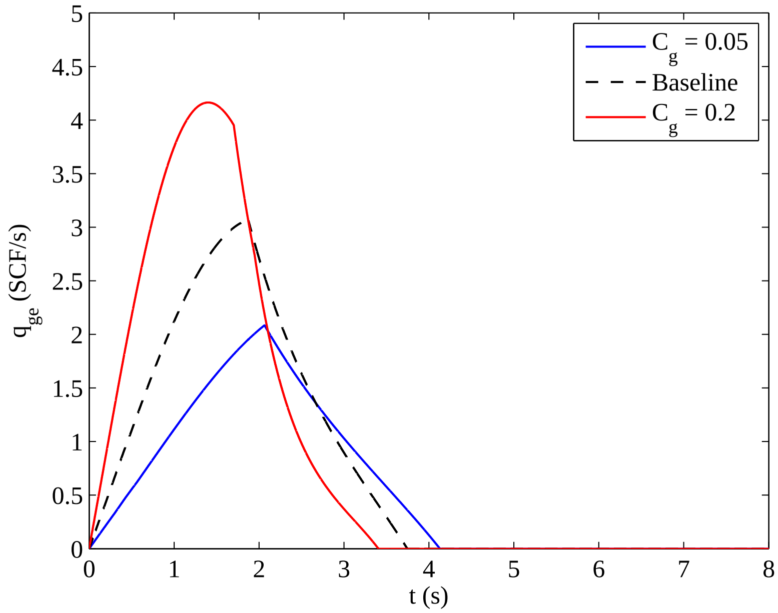

Figure 27: Baseline values with varied C_g, gas outflow during purge

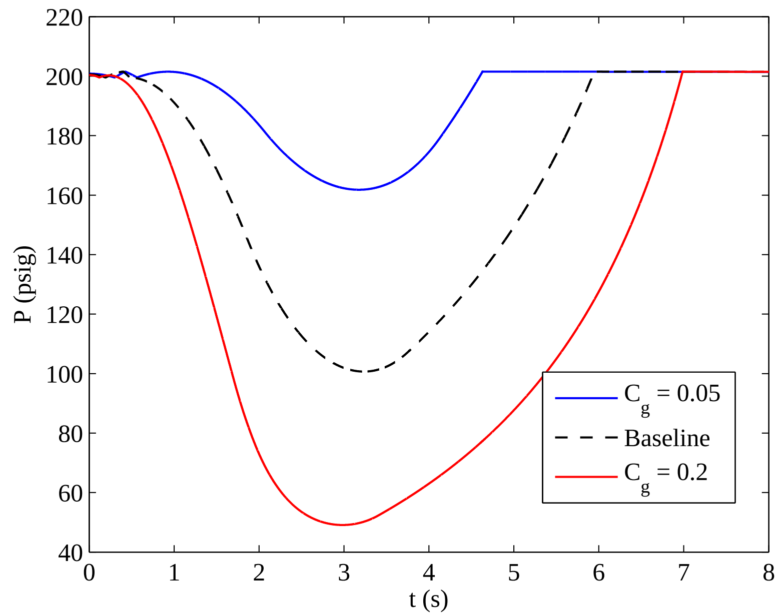

Figure 28: Baseline values with varied C_g, gas pressure during purge

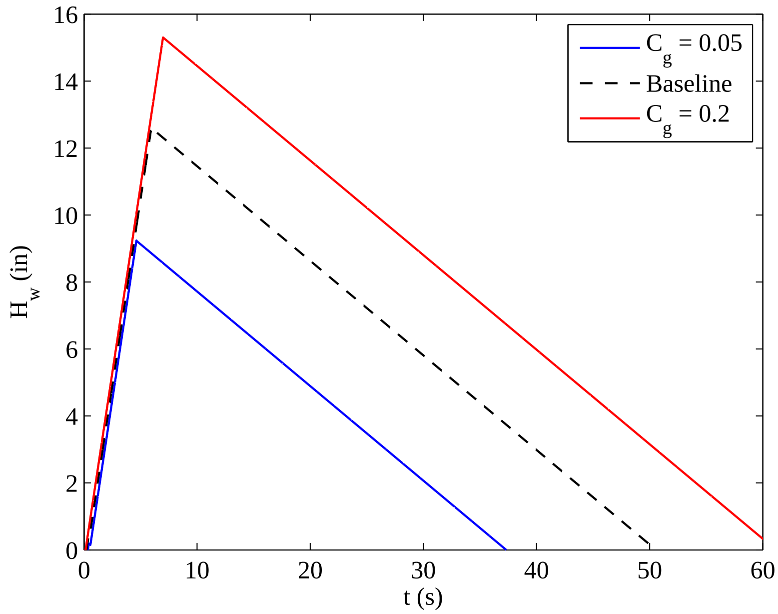

Figure 29: Baseline values with varied C_g, gas-liquid level during purge

the figure, two representations are compared side-by-side. The sole distinction is the orientation of the inlet pipe. In configuration A, the outward normal of the inlet face points in the $+z$ direction. In configuration B, the inlet pipe is rotated 180^o about the y-axis, and the inlet face normal is directed along the $-z$ direction. Each configuration is simulated with a single case that corresponds to a inflow mixture composed of 1000 bbl/day water and 200 MSCF/day gas. In both configurations, the CFD domain has a single inlet and a single outlet. The multiphase mixture flows through the inlet, while only the liquid phase water exits the domain through the outlet. Therefore, the CFD simulation represents the gas expansion process as described in the section 2.

As shown in the geometry graphic in figure 30, the entire domain is utilized in the simulation. During initial investigations of the CFD analysis, it was determined that the whole domain was required to accurately capture the phase separation. The pressure connection between the tank and stack as provided by the inner-pipe proved difficult to accurately model without a physically realistic configuration. Because of this choice, the grid resolution is kept relatively coarse in these preliminary runs. Figure 31 provides a visual representation of the coarsest grid. In areas of high fluid velocity or liquid-gas interaction, the grid is refined to yield improved physical accuracy at a limited computational expense.

Figure 32 displays contours in the $x-y$ plane of the gas volume fraction (VF) a few seconds into the simulation. As displayed, the blue areas represent zero VF (all liqiud), and the red represents unity VF (all gas). The geometry shown is configuration A from the left side of figure 30, and the inlet is oriented out of the page in figure 32. Visible in the figure, there is a pocket of gas contained at the top of the tank at the weld-cap. The tank to stack connection of the inner pipe is not shown in figure 32, but the gas is transferred to the central stack at exits near the top. Within the stack, the liquid-gas interface is located about sixteen inches from the top. Volume renderings

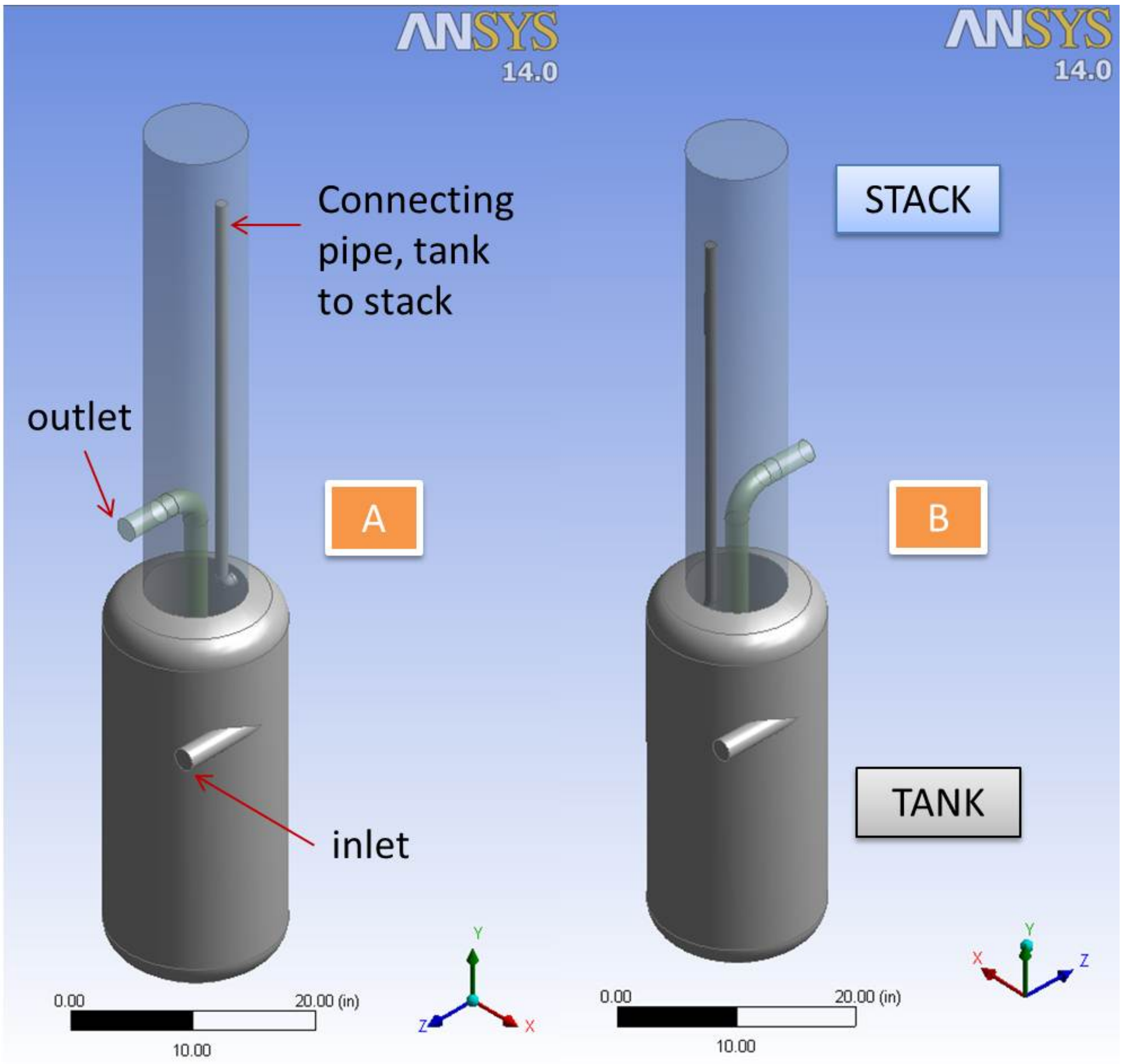

Figure 30: Comparison of two geometries used in CFD

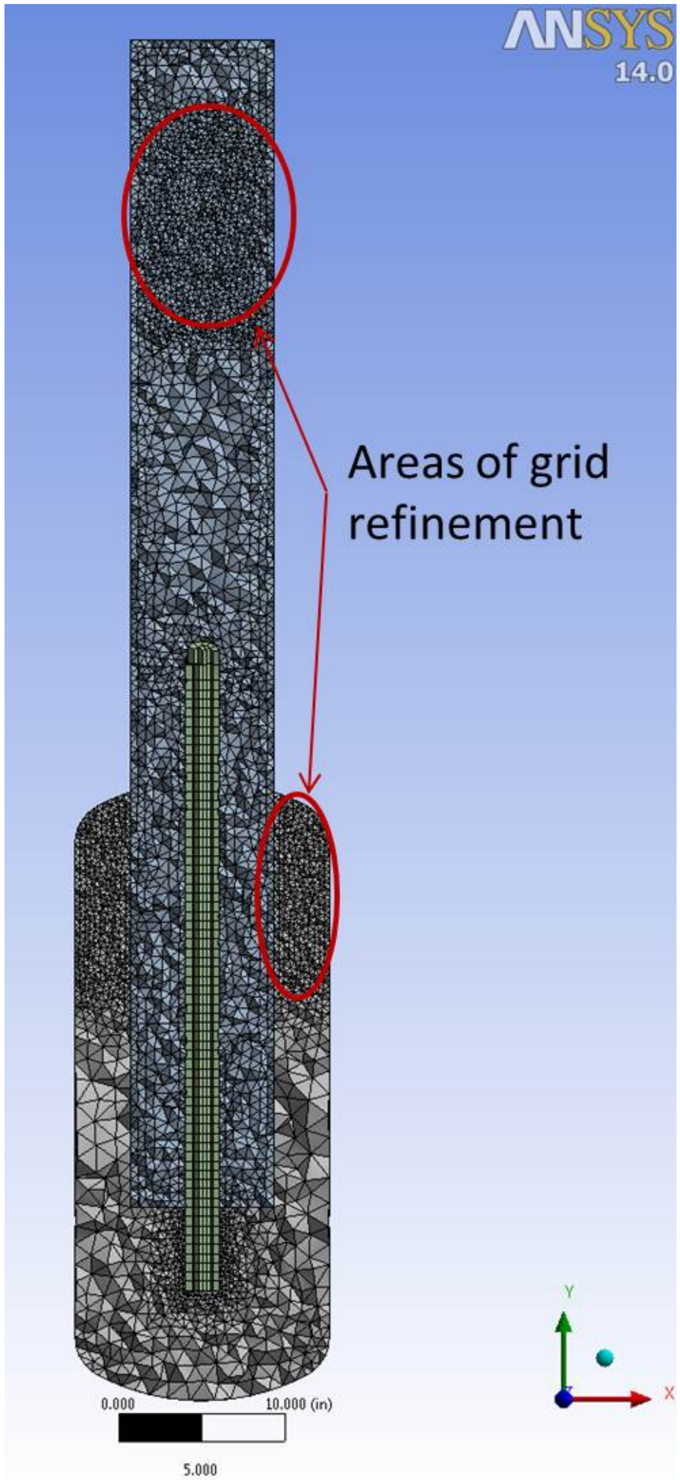

Figure 31: Mid-section slice showing unstructured grid and areas of increased resolution

of VF are shown in figure 33, which provides a side-by-side comparison of the two configurations. In these images, the negligible values of VF (liquid phase) are made transparent for enhanced stability through the volume. Evident in the frames, there is a slight difference in the amount of gas transferred from the tank to the stack. A single-frame interpretation is misleading, though, because figure 34 shows the same simulation two seconds later and the balance has reversed. At later time, configuration B in the right-hand frame shows less gas remaining in the tank.

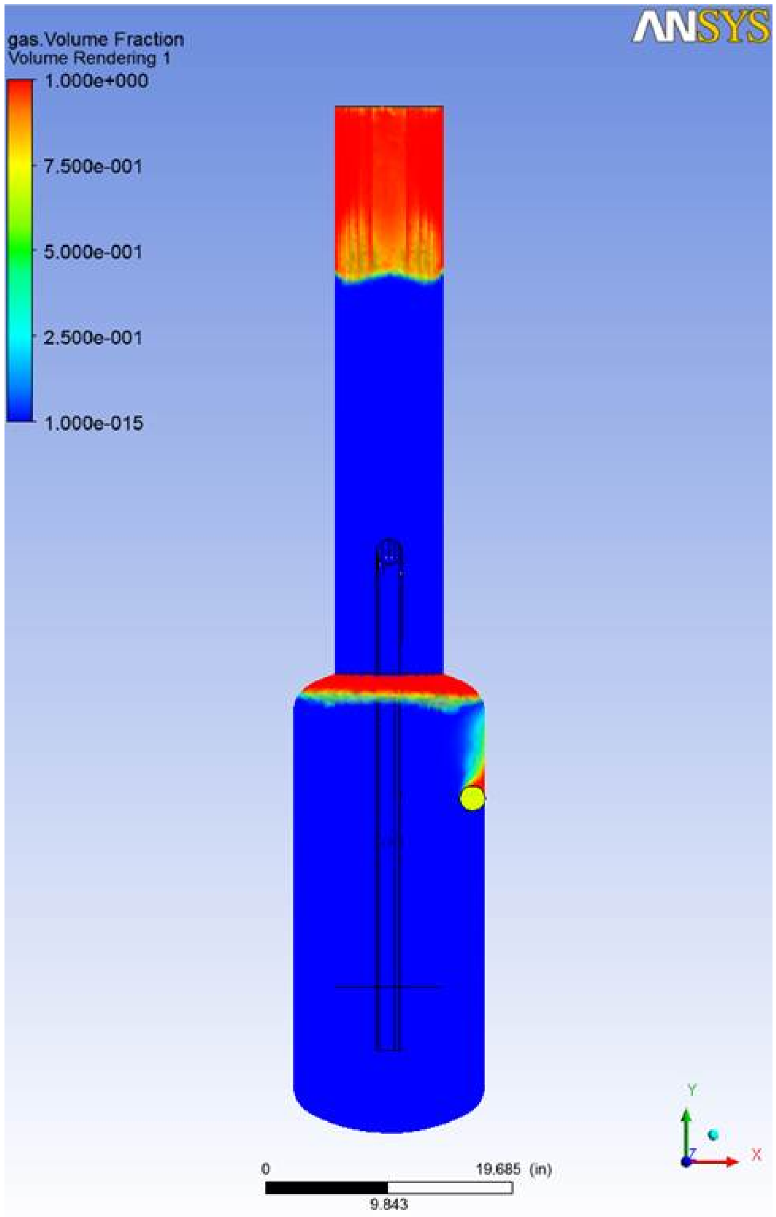

Figure 32: Configuration A, gas volume fraction contours at $t = 2.0\,\mathrm{s}$

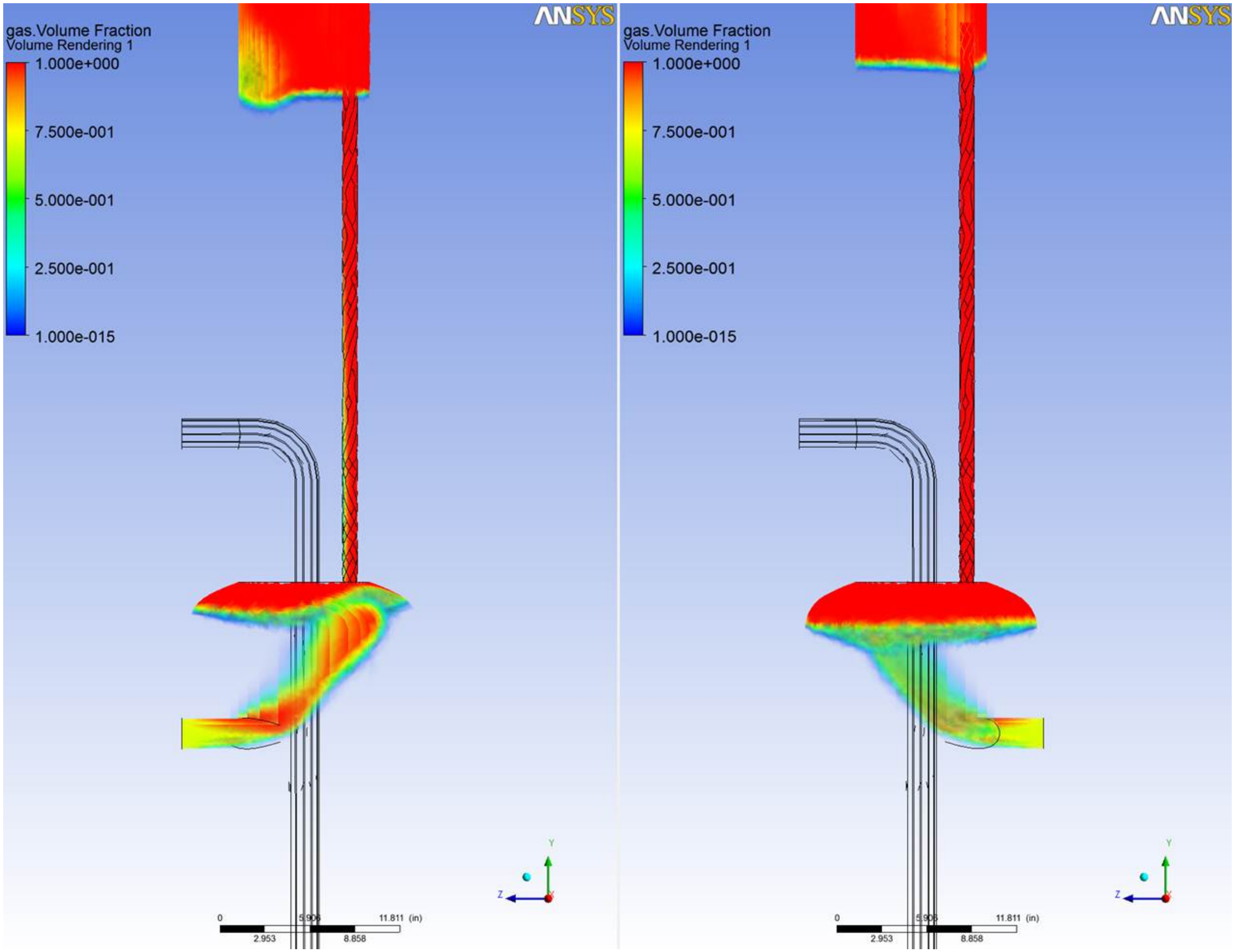

Figure 33: Both configurations (A on left, B on right) with identical camera views, gas volume fraction contours at $t = 2.0\,\mathrm{s}$

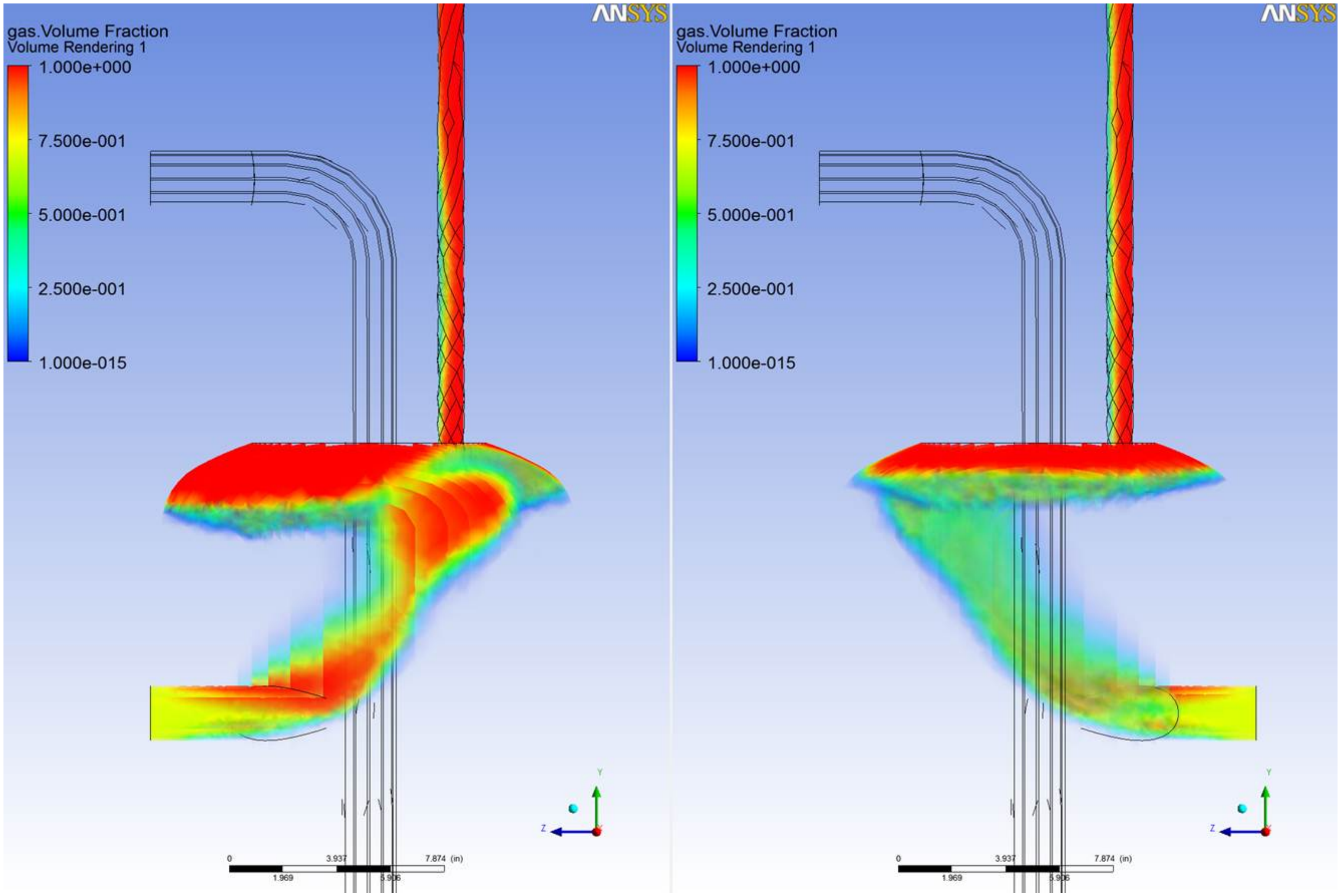

Figure 34: Both configurations (A on left, B on right) with identical camera views, gas volume fraction contours at $t = 4.0\,\mathrm{s}$

Unfortunately, there is no good physical explanation available at this time. However, intuitive reasoning would lead us to suspect the primary distinction between the two configurations is the fluid velocity of the mixture as it swirls around the top of the tank. At the face of the inner-pipe, the tangential fluid velocity is higher in configuration A. Gas delivery to the inner-pipe of configuration A is accelerated in the early stage of the simulation due to the proximity of the inlet. In contrast to the 90^o degrees of angular travel for configuration A, the mixture must travel 270^o in configuration B. At later times, the gas delivery through the inner-pipe may be increased in configuration B because of the lower fluid velocity. Moreover, the early time stages should probably be ignored as they represent a necessary transient of the simulation but do not provide a physical reflection of the quasi-steady inflow under operating conditions.

4 Summary

Two separate phases of investigation were performed and presented in this report. Both should be considered as preliminary work, where validation and interpretation work remains to be completed at a future stage. In section 2, a one-dimensional thermodynamic analysis was applied to capture the operating cycle of the device. Three processes of gas purge, compress, and expand comprise the complete cycle. Equations of mass conservation and state were applied and solved numerically. The results demonstrate adequate capture of the primary physical mechanisms, and such analytical work provides a useful tool upon calibration with known results or measurements. A calibrated model could be leveraged for design optimization and identification of operating conditions requiring deeper investigation. In section 3, a three-dimensional transient CFD simulation was performed at coarse resolutions to verify the proper application of boundary conditions and turbulence modeling. While it is too early to interpret the results, the preliminary CFD investigation reveals possible effects of pipe-pipe orientation.

In closing, the device is known to be an effective tool for the gas-liquid phase separation. Although simple in design, the analysis proves challenging to model and simulate due to the interactions of phases and processes spawned by control devices. We would look forward to future work towards improving the existing analysis presented here plus the possibility of a few items from a brief list below containing a few ideas for further study.

- Calibrate 1d models (*e.g.* , C_g, and K_w) with field measurements
- Towards the above items, perform field experiments to measure transient pressure
- Improve the applied 1d model for back-pressure and check valve operation
- For above item, a laboratory experiment involving a simple flow loop could allow relatively simple characterization
- Examine effects of early check valve opening ($P_c < P_{set}$)
- Examine temperature effects, ambient and mixture
- Derive a measure of efficiency, perhaps relating amount of gas processed to required pump power
- Examine effects of time-varying inflow

- Include and quantify effects of injecting noise into system inputs and signals
- Investigate optimization possibilities, *e.g.* influence of nonlinear gas valve actuation

The author acknowledges the NMSBA and Muleshoe Engineering for their assistance and support on this project.

Nomenclature

δ_f	Linear travel between on-off positions in float switch
$\dot{m}_{ge}$	Mass outflow rate of gas
$\dot{m}_{gi}$	Mass inflow rate of gas
$\dot{m}_{we}$	Mass outflow rate of water
$\dot{m}_{wi}$	Mass inflow rate of water
γ	Polytropic gas process exponent
τ_v	Gas valve open-close time delay
A_g	Representative area of gas exit piping
C_g^*	Discharge coefficient, gas exit
C_g	Secondary discharge coefficient, gas exit (choked)
H_f	Distance to median float level, relative to top cap
$H_g(t)$	Gas-liquid interface height, relative to top cap
$H_w(t)$	$H_f^+ - H_g$, Gas-liquid interface level, distance relative to float open position, $H_f + 0.5\delta_f$
k	Gas specific heat ratio (c_p/c_v)
K_w	Back-pressure valve proportional response constant, water exit
P_g^*	Absolute choke pressure
$P_g(t)$	Absolute pressure of gas gathered in vessel stack
P_i	Absolute pressure of mixture input
P_{set}	Absolute pressure downstream of water check valve (*back pressure*)
P_{sink}	Absolute pressure downstream of gas release valve (*sink pressure*)
q_{ge}	Volume outflow rate of gas (standard conditions)
q_{gi}	Volume inflow rate of gas (standard conditions)
q_{we}	Volume outflow rate of water

q_{wi}	Volume inflow rate of water
T_i	Temperature of mixture input
V_f^+	Occupiable volume at float open (low) position
V_f^-	Occupiable volume at float close (high) position
V_f	Occupiable volume at float median position, H_f
$V_g(t)$	Volume of gathered gas